



The impact of ERA-Interim winds on wave generation model performance in the Southern Caspian Sea region

Majid Noranian Esfahani¹ · Mahmood Reza Akbarpour Jannat¹  · Babak Banijamali² · Seyed Mostafa Siadatmousavi³

Received: 19 November 2016 / Accepted: 27 August 2018 / Published online: 4 September 2018
© Springer-Verlag GmbH Austria, part of Springer Nature 2018

Abstract

The aim of the present work is to evaluate wind dataset in generation of the wave characteristic along the southern basin of the Caspian Sea (SBC). To achieve this purpose, satellite altimetry data, numerical model results and field measurements were considered for 2011. The mixed re-analysis/forecast wind data from European Center for Medium Range Weather Forecast, ERAI_MIXED, are analyzed. Comparisons are made using altimetry data from CERSAT, mixed re-analysis/forecast GFS datasets (GFS_MIXED) and field observation from two buoys and one ADCP located in SBC. The modeling was carried out using the SWAN model over a composite-overlap nested grid system. The results showed that the ERAI_MIXED underestimated wind data in SBC, similar to other datasets from ECMWF and GFS. However, the simulation results implied that using the same configuration for the wave model, ERAI_MIXED led to superior results compared to GFS_MIXED and ERAI_MIXED-COR. Comparison with limited observation showed that ERAI_MIXED data slightly overestimated the wave height in the offshore station and underestimated it at the nearshore buoy. Finally, model results showed that moderate to low wind speed over the SBC might generate the waves up to 4 m wave height.

1 Introduction

Knowledge of bulk wave parameters is essential in engineering activities over the continental shelf from offshore to the surf zone. Predicting wind-induced waves is highly associated with the accuracy of the wind data forced into the model (Zhao and Toba 2001). The wind forcing can be provided from the measurement systems or global weather datasets. Engineers prefer to use the result of numerical weather prediction model because of scarce and irregular measurement network and exorbitant costs of field measurements. The major efforts are concentrated to use the global atmospheric model databases such as European Centre for

Medium-Range Weather Forecasts (ECMWF) and Global Forecast System (GFS). These databases cover more than 50 years of met-oceanic information; however, there is still some hesitation for choosing them in the Caspian Sea (Hartgerink 2005; Mazaheri et al. 2013).

It is important to achieve an accurate prediction of nearshore waves in the southern part of the Caspian Sea where rip current generated by waves is drowning up to 500 people per year. The weather climate substantially changes from south to north of the Sea. The Southern part is affected by Mediterranean tropical fronts, which cause hot and dry summers and warm winters. Over the north of Caspian Sea, the weather is dominated by the Azores high pressure that causes summer-time northerly winds and by the Asiatic anticyclone which creates a winter-time easterly cold winds (Graham et al. 2002). In the southern part of the Caspian Sea, the annual cycle of the monthly mean wind produced from the global atmospheric models represents northward winds during December and January, south-southwestward divergence winds during February–July, and westward winds through August–November (Ibrayev et al. 2010). The reversal wind field as a result of the reversed land-sea temperature differences between the austral summer and winter (Ibrayev et al. 2010) leads to seasonal changes in wave

Responsible Editor: F. Mesinger.

✉ Mahmood Reza Akbarpour Jannat
akbarpour@inio.ac.ir

¹ Iranian National Institute for Oceanography and Atmospheric Sciences, Tehran 14118-13389, Iran

² Darya-Bandar Consulting Engineers, Tehran 16677-39113, Iran

³ Iran University of Science and Technology, Tehran 16846-13114, Iran

pattern. Therefore, a precise knowledge of wind field data is required for modeling the bulk wave parameters.

In contrast to studies of other coastal processes, there are few studies focused on wave modeling in the southern part of the Caspian Sea. In most of these cases, data assimilation was a major concern. Lopatoukhin et al. (2004) offered some results for obtaining the wind and wave climate close to Russia from the National Centers for Environmental Prediction-National Center for Atmospheric Research (NCEP/NCAR) re-analysis dataset. They modified the dataset according to the Markov processes (Parzen 1999) using 280 thousand ships observations in the Caspian Sea, which were available since 1948. Moreover, an improved wind data set was utilized as the input of SWAN (Simulating Wave Nearshore) model (Booij et al. 1996). Their results showed a periodic spatiotemporal variability in the weighting coefficients. Hartgerink (2005) also applied the NCEP wind database in combination with SWAN model and discovered NCEP wind database does not contain sufficient information on the high-frequency wind speed variations which are needed to determine the design wave height. Additionally, he found that unlike the southern basin of the Caspian Sea (SBC), swells do not play an important role in the Northern part. Furthermore, it was proposed that the measured spectra from the Caspian Sea may be adequately described by the theoretical JONSWAP and TMA spectra. Golshani et al. 2007 did the 11 years (1992–2002) of wave simulation in the Caspian Sea to achieve the wave climate atlas of the basin. ECMWF operational wind field with spatial resolution of 0.5° and temporal resolution of 6 h was modified based on comparison with in situ and satellite input. This modified ECMWF operational wind input was used in Kamranzad et al. (2016) study as well. Hadadpour et al. (2013) simulated the wave bulk parameters using SWAN in the Anzali port region, situated at the southwestern part of the Caspian Sea. They forced the model using QuikSCAT wind field and applied an artificial neural network to the simulated wave parameters to improve model performance. Mazaheri et al. (2013) verified ERA-40 wind components using QuikSCAT satellite measurements and applied ERA-40 wind field with a $0.5^\circ \times 0.5^\circ$ horizontal resolution over the Caspian Sea for a period of 32 years. They proposed correction factors for wind to improve simulation results from SWAN. Their results implied that the correction of eastward wind components is needed over the entire basin whereas for the northward components, the modification is only needed for the SBC. Although they reported some differences between the ECMWF wind field and QuikSCAT wind measurements, they did not provide any information about the corrected and pure ECMWF wind field. Rusu and Onea (2013) evaluated the wind and wave energy resources along the Caspian Sea for allocating turbine farm. Satellite data were provided from Archiving, Validation and Interpretation of Satellite

Oceanographic (AVISO) data and model results were provided by SWAN model using a staggered grid which was forced by $1.5^\circ \times 1.5^\circ$ ECMWF wind data. Hadadpour et al. (2014) used SWAN model for simulating the wave characteristics over a nested grid system to describe the existence and variability of wave energy along the Anzali coasts. Similar to the present study, they used a nested procedure to obtain optimal results at both global Caspian Sea domain and the coastal Anzali domain. Kamranzad et al. (2016) evaluated the wave energy potential and its spatial and temporal variations in the SBC. They used SWAN model to hindcast wave characteristics for a period of 11 years using the modified ECMWF operational wind data (Golshani et al. 2007) and found that southwestern part of the Caspian Sea is less energetic than other areas.

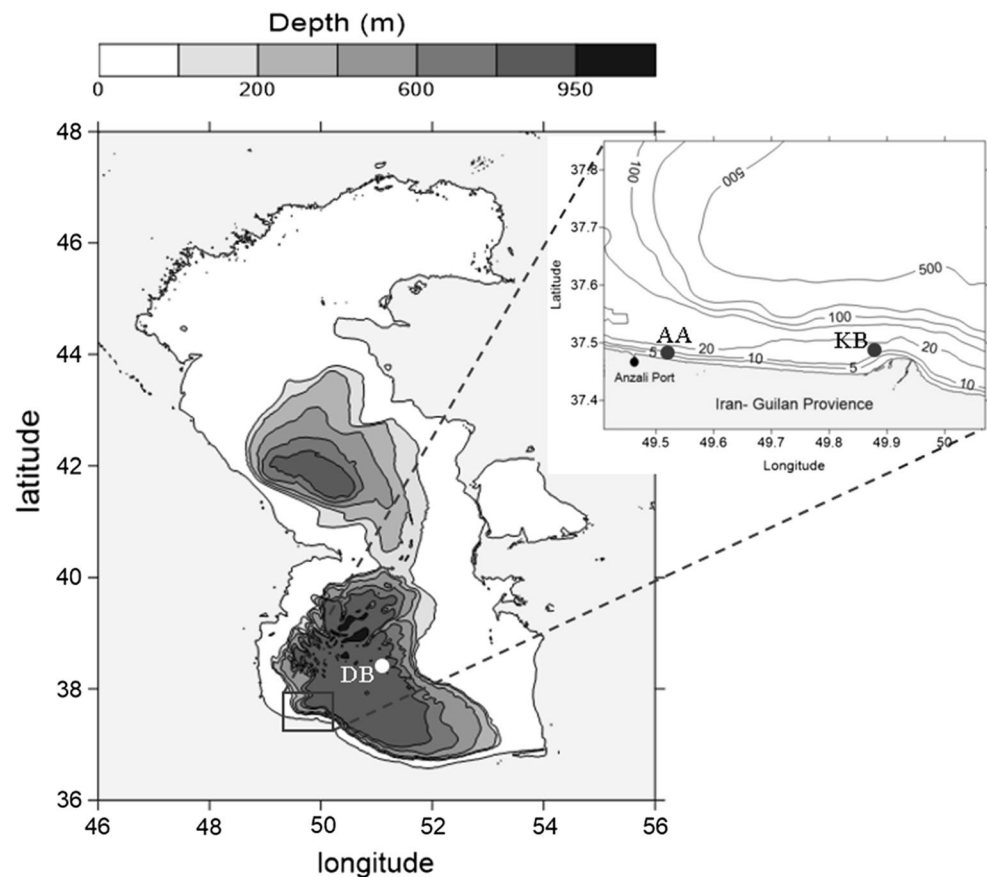
The latest released dataset from ECMWF which called ERA-Interim (ERA-I) is probably more interesting for researchers than NCEP/NCAR and ERA-40 datasets. Evaluation of the wave characteristics using this dataset is still an open issue in many water bodies around the world. The main objective of this study is to evaluate ERA-I over the southern part of the Caspian Sea.

To accomplish the present work, SWAN model was used in two-layer nested grids by the ERA-I forcing in order to determine the bulk wave parameters in SBC. The field of study is described in the following section. Data sets, underlying physics, model configuration and statistical indices are presented in Sect. 3. Validating wind datasets based on remotely sensed data, analyzing ERA-I and GFS wind datasets based on buoy measurements, and also bulk wave characteristics based on buoy measurements. The modeling results are presented in Sect. 4 and followed by the conclusions of the study.

2 Field of study

Caspian Sea extends between 46.67°E to 54.80°E and 36.56°N to 47.1°N with three meridional interconnected regions (Fig. 1): the shallow Northern Caspian Basin (NCS), the deep Middle Caspian Basin (MCB) and the deeper Southern basin of the Caspian Sea (SBC) with the maximum depth of 25, 778 and 1025 m, respectively. In the northern part, the depth noticeably increases towards MCB, where the average depth is 190 m. The SBC is being separated from the MCB by the Apsheron Rift. The optimum values for the geometry of the continental shelf are found to be up to 11 km and 1° for the width and slope close to the Derbent and Divichi, expanding to the south where the continental shelf slope becomes sloping downward (Naseka and Bogutskaya 2009). Based on the bathymetric data in each part of the Caspian Sea, the mean slope of sea-bed locally changes from mid-shelf to the coastline. Forty-six

Fig. 1 Bathymetrical map of parent and child grids implemented for the coupled model. The position of deep and shallow buoys and ADCP station are shown. Contour levels are given in meters



percent of sea area lies on the shelf with depths up to 100 m, while the continental slope of the SCB is indeed quite steep, with the eastern side slope running deeper and wider than the corresponding values on the western side (Naseka and Bogutskaya 2009). Historically, the Caspian Sea level (CSL) has experienced long- and short-time fluctuations; however, these have been limited between -25 to -29 m below the open-ocean surface since 1995 (Arpe and Leroy 2007). In 2011, the CSL was -28 m below open sea datum. Bathymetry data for simulations in this study were generated from General Bathymetric Chart of the Oceans (GEBCO) database with 30 s horizontal resolution which is available from <http://www.gebco.net>.

3 Data and methodology

3.1 Datasets

Historical met-ocean data measurements are scarce in SBC along the Iranian coasts. Port and Maritime Organization (PMO) have implemented a national monitoring project for the southerly coast of the Caspian Sea since 2007. In addition, a set of ADCP measurements has been conducted along

its inner-shelf by Iranian National Institute for Oceanography and Atmospheric Sciences (INIOAS).

For this study, wind measurements are collected from two oceanic buoy which have been deployed in center of SBC (DB) from February to November 2011 and in mid-shelf near Kiashahr Port (KB) from March 2010 to May 2011. The wave characteristics have been measured by above-mentioned buoys (DB and KB) and an ADCP which have been conducted from 27 June to 10 July 2011 close to the Anzali Port (AA). The spectral wave data were not available from the buoys due to memory limitation of the instrument. Deployment depth and geographic positions are presented in Table 1 and shown in Fig. 1.

In addition to buoys observation, the atmospheric forcing is taken from ECMWF and GFS datasets. Both of them are released in re-analysis (RE-ANL) and combination of re-analysis and forecast (MIXED) forms on multiple scales. The re-analysis data include results at 0000, 0600, 1200 and 1800 UTC, and the mixed one includes both re-analysis fields (at 0000, 0600, 1200 and 1800 UTC) and forecast fields (at 0300, 0900, 1500, 2100 UTC).

ECMWF provides weather information from 1979 to 2017 using six different re-analysis products. The first, ERA-15, is 15 years generated re-analyses data which covers from 1979 to 1993. The second one, ERA-40, covers up

Table 1 Deployment depth and geographic position of measurement instruments (after PMO and INIOAS)

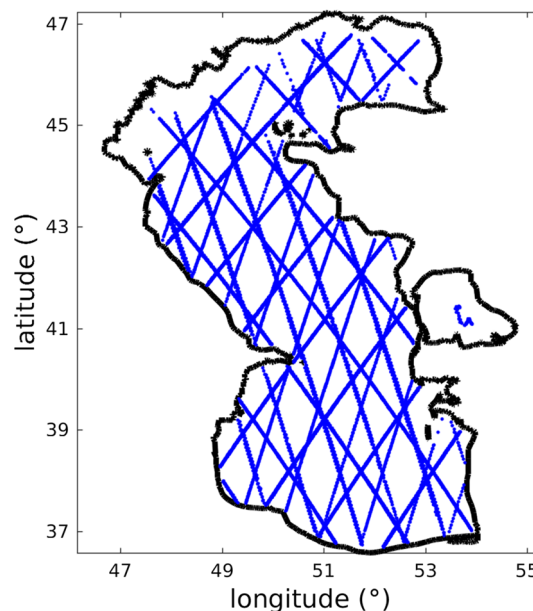
Data owner	Device type	Station name	Station depth (m)	Longitude (°E)	Latitude (°N)	Available data
PMO	Buoy	DB	800	51.20	38.39	Wind + wave
PMO	Buoy	KB	14	49.87	37.49	Wind + wave
INIOAS	ADCP	AA	8	49.52	37.48	Wave

to 45 years from the International Geophysical Year (1957) to 2002. The third, ERA-Interim Re-Analysis (ERA-Interim), is a re-analysis product for replacing ERA-40, which is available since 1979. ECMWF also released three new re-analysis datasets, spanning 1900–2010 which known as ERA-20C, ERA-20CM and CERA-20C datasets. The ERA-Interim atmospheric model is natively running under 256×512 latitude/longitude horizontal grid, which means about 0.75° horizontal grid resolution at the equator. ERA-Interim Ocean-Wave model results are stored on the 1.0° latitude/longitude grid. ERA-Interim data can optionally interpolated to a custom grid and same horizontal resolution in both directions. The default interpolation method is bilinear for continuous fields (e.g., wind velocity components) and by nearest-neighbor for discrete fields (e.g., wave 2D spectra).

For obtaining wind data, re-analysis and the mixed re-analysis/forecast datasets, ERA-Interim with 0.5° , ERA-Interim Mixed with 0.125° , and GFS Mixed with 0.5° horizontal resolutions are considered. Also, we examined ERA-Interim Mixed-COR with 0.125° resolution which has been corrected the northward and eastward wind components as suggested by Mazaheri et al. (2013).

All wind datasets provide the wind components at 10 m above the sea surface, which are spatially distributed on a regular rectangular grid. The near-surface wind transferred to the wave model curvilinear grids using ROMS MATLAB scripts distributed along with the pre-/post-processing ROMS MATLAB toolbox, available from <https://www.myroms.org/svn-/src/matlab>.

For choosing the best dataset, all wind datasets and the corresponding simulated wave characteristics were compared with remotely sensed data from CERSAT. These data were obtained from the Centre de Recherche et d'Exploitation Satellitaire (CERSAT), at Ifremer, Plouzané (France). They were produced in the framework of GlobWave project, funded by the European Space Agency (ESA). It is combination of satellite wind data from ERS2, ENVISAT, JASON1, JASON2 and CRYOSAT1 during 2011. Figure 2 shows satellite track paths over the Caspian Sea including 27,852 data points in 2011. Since data from neighboring points are not statistically independent, they cannot be used for statistical analysis; therefore, all data points cannot be used to calculate statistical indices. To remedy this problem, only points which are measured at

**Fig. 2** Combination of track paths of ERS2, ENVISAT, JASON1, JASON2 and CRYOSAT1 satellites during 2011 over the Caspian Sea

least 20 min apart in time and 25 km apart in space were used, reducing the dataset to 6977 points. We considered data in SBC with latitudes less than 40.5° and, as a result, there were 2877 data points available. The data from ERA-Interim dataset were temporally and spatially interpolated at those points.

3.2 Model configuration

The SWAN model is used for evaluating the response of the wave model to ERA-Interim wind forcing. The model can employ a rectilinear, a curvilinear or an unstructured grid. Furthermore, nested computing can be supported for structured grids. To provide a better spatial resolution close to the observation stations, a two-level composite nesting curvilinear grid system was created. The nesting technique provides two benefits: it reduces the computational cost in unconcerned areas and it provides accurate results close to in situ measurements. The regional (parent) and local (child) domains are built based on the GEBCO 30 arcsec data. Since the resolution of GEBCO data is not sufficient for modeling coastal waters, sounding bathymetric data

surveys—provided by INIOAS—merged into the GEBCO bathymetric data. Horizontal resolution is 2×2 km for the parent grid and it is defined with 7:1 refinement factor for the child grid. The child grid resolution is 300×300 m, encompassing the Guilan province (Fig. 1), and spans from 49.4°E to 50.1°E and from 37.35°N to 37.85°N .

SWAN model solves the spectral wave action balance equation (Hasselmann et al. 1973) with sources or sinks terms for wave energy density, including generation, dissipation, and transfer processes. It represents the linear and exponential growth by the wind, dissipation due to whitecapping and bottom friction, depth-induced wave breaking and energy transfer due to quadruplet and the triad wave-wave interaction (Booij et al. 1999). The following configuration has been used for this study: linear wind wave generation was incorporated using the formulation of Cavaleri and Rizzoli (1981). The third-generation mode (GEN3) for exponential growth of waves under wind force was employed using WAM cycle 3 formulation. Calculation of whitecapping was based on formulation provided by Hasselmann (1974) and can be applied according to Komen et al. (1984). Different values for the whitecapping coefficient (C_{ds}) were used for tuning the wave parameters. The treatment of the energy dissipation due to the depth-induced breaking which has a significant effect on wave properties in nearshore areas was based on Battjes and Janssen (1978). In the present study, a constant breaker index was used with values of 0.73 and 1.0 for the ratio of maximum individual wave height over depth and tuning coefficient on the rate of dissipation, respectively. Wave energy is dissipated by the bottom friction according to the following formulation:

$$S_{ds,b} = -C_b \frac{\sigma^2}{g^2 \sinh^2 kd} E(\sigma, \theta), \tag{1}$$

where C_b is the bottom-friction coefficient. Based on JONSWAP experiments, Hasselmann et al. (1973) estimated a constant value of $0.038 \text{ m}^2/\text{s}^3$ for swell dissipation. Bouws and Komen (1983) suggested a value of $0.067 \text{ m}^2/\text{s}^3$ for fully developed wind seas. For a more realistic condition, bottom-friction coefficient is related to bottom-orbital velocity U_{rms} :

$$U_{rms}^2 = \int_0^{2\pi} \int_0^\infty \frac{\sigma^2}{g^2 \sinh^2 kd} E(\sigma, \theta) d\sigma d\theta, \tag{2}$$

Based on Collins description (Collins 1972):

$$C_b = C_f g U_{rms}. \tag{3}$$

Therefore, the bottom-friction coefficient is not constant according to Eq. (3) and it depends on the speed of the orbital wave. For including the effects of bottom friction dissipation, expression (3) was activated using $C_f=0.015$ for the bottom friction coefficient.

The shape of the wave spectrum is mainly controlled by nonlinear wave-wave processes (Hasselmann et al. 1985).

Wave-wave interactions illustrate different behavior in deep and shallow waters. In deep water condition, quadruplet wave-wave interaction transfers the wave energy from the spectral peak to lower and higher frequencies, especially during wave growth. SWAN computes quadruplet wave-wave interaction using the discrete interaction approximation (DIA) proposed by Hasselmann et al. (1985) for multidirectional waves. Close to the shore and in very shallow water, triad wave-wave interactions become important for steep waves. This process transfers energy from the peak frequency to its harmonics (Beji and Battjes 1993) which is computed in SWAN by the lumped triad approximation (LTA).

3.3 Statistical indices

Statistical parameters can be used for evaluating the quality of wind datasets and the performance of wave model. Following Wilks (2011), in this study, mean bias error (MBE), root-mean squared error (RMSE), correlation coefficient (CC) and scatter index (SI) were used:

$$MBE = \left[\sum (A - A_{obs}) \right] / n, \tag{4}$$

$$RMSE = \sqrt{\left[\sum (A - A_{obs})^2 \right] / n}, \tag{5}$$

$$CC = \frac{n \sum A A_{obs} - \sum A \sum A_{obs}}{\sqrt{\left[n \sum A^2 - (\sum A)^2 \right] \left[n \sum A_{obs}^2 - (\sum A_{obs})^2 \right]}}, \tag{6}$$

$$SI = \frac{RMSE}{\sum A_{obs}}. \tag{7}$$

The index of agreement (IA) is another useful statistical parameter used for quantifying the agreement between simulated and observed values (Willmott et al. 2012):

$$IA = 1 - \frac{\left[\sum (A - A_{obs})^2 \right]}{\left[\left| \sum A - \frac{(\sum A_{obs})}{n} \right| + \left| \sum A_{obs} - \frac{(\sum A_{obs})}{n} \right| \right]^2}. \tag{8}$$

Table 2 Statistical comparison of CERSAT dataset ($U10_{SAR}$) vs. (a) ERAI_RE-ANL, (b) ERAI_MIXED, (c) ERAI_MIXED-COR, and (d) GFS_MIXED datasets in SBC, in terms of mean bias error (MBE) and root mean square error (RMSE), scatter index (SI), correlation coefficient (CC) and index agreement (IA)

	MBE (m/s)	RMSE (m/s)	SI	CC	IA
$U10_{ERAI_RE-ANL}$	-0.86	2.15	0.27	0.71	0.80
$U10_{ERAI_MIXED}$	-0.69	1.60	0.28	0.68	0.79
$U10_{ERAI_MIXED-COR}$	-0.13	1.76	0.31	0.68	0.82
$U10_{GFS_MIXED}$	0.02	1.86	0.33	0.70	0.84

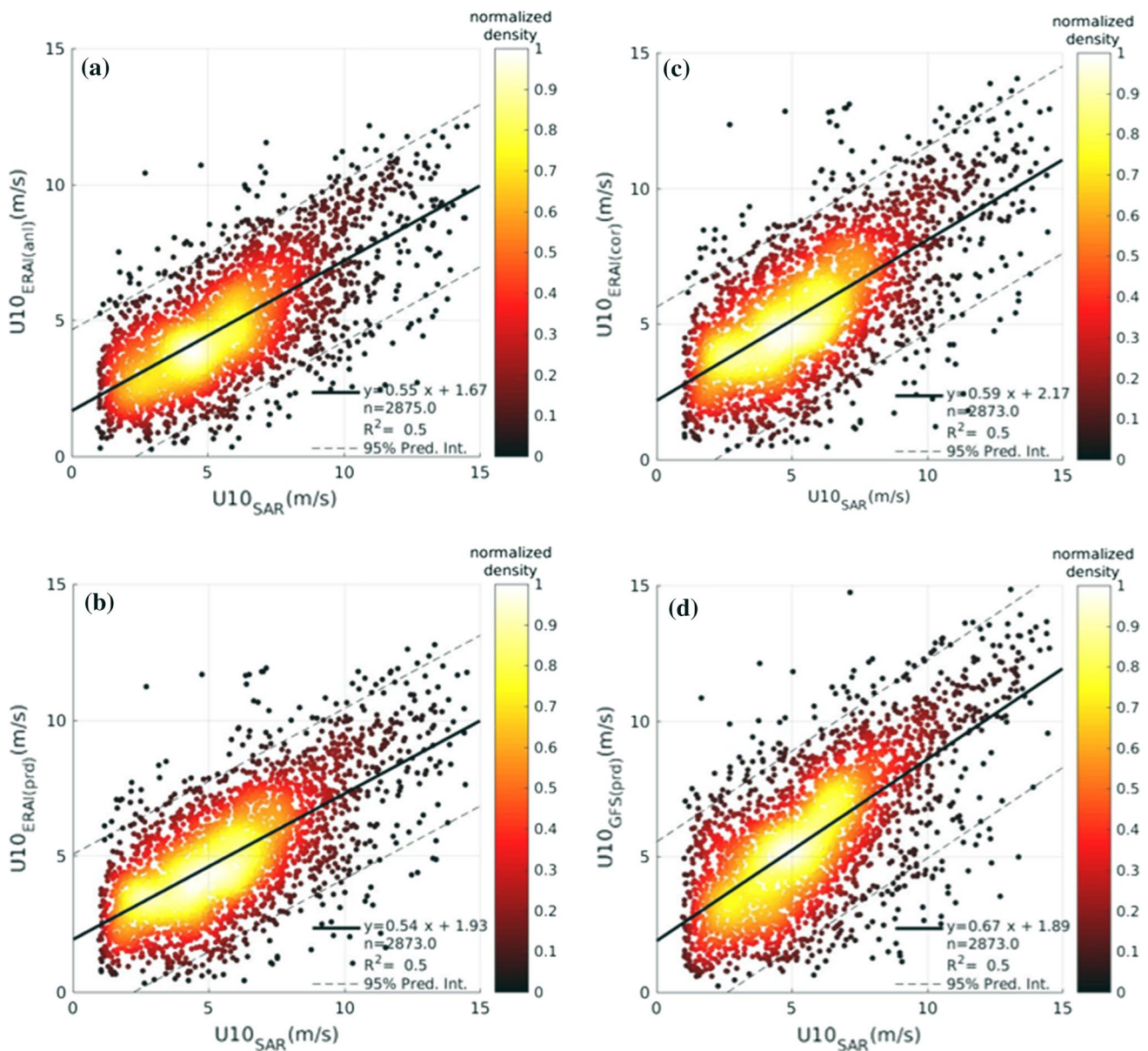


Fig. 3 Quantile–quantile scatter plot of wind speed from CERSAT dataset ($U10_{SAR}$) vs. **a** ERAI_RE-ANL, **b** ERAI_MIXED, **c** ERAI_MIXED-COR, and **d** GFS_MIXED datasets

The MBE describes the average difference between the ERAI and buoy data. Here, the negative MBE values suggest the averages amount of underestimation in the ERAI values, while the positive values indicate overestimation. The RMSE describes how close measurements and model data are, and a lower value of RMSE implies a better agreement between the ERAI and buoy data. The ideal values of MBE and RMSE are zero. The SI determines the percentage of expected error for the model parameter, and a smaller value indicates a better agreement. Finally, the closer the value of IA to 1, the better the agreement between model results and observations.

4 Results and discussion

4.1 Validating wind datasets

European Centre for Medium-Range Weather Forecasts has produced the ERA-Interim dataset in multiple scale in space and time interval as well as GFS from NCEP/NCAR. To obtain more accurate wind dataset, the ERAI_RE-ANL, the ERAI_MIXED and ERAI_MIXED-COR datasets are compared with CERSAT wind data ($U10_{SAR}$) in SBC. The results are also compared with data from GFS_MIXED wind dataset.

Fig. 4 Comparison of the wind components of u and v , and $U10$ from the observation and ERAI_ER-ANL, ERAI_MIXED, ERAI_MIXED-COR and GFS_MIXED data offshore buoy (DB)

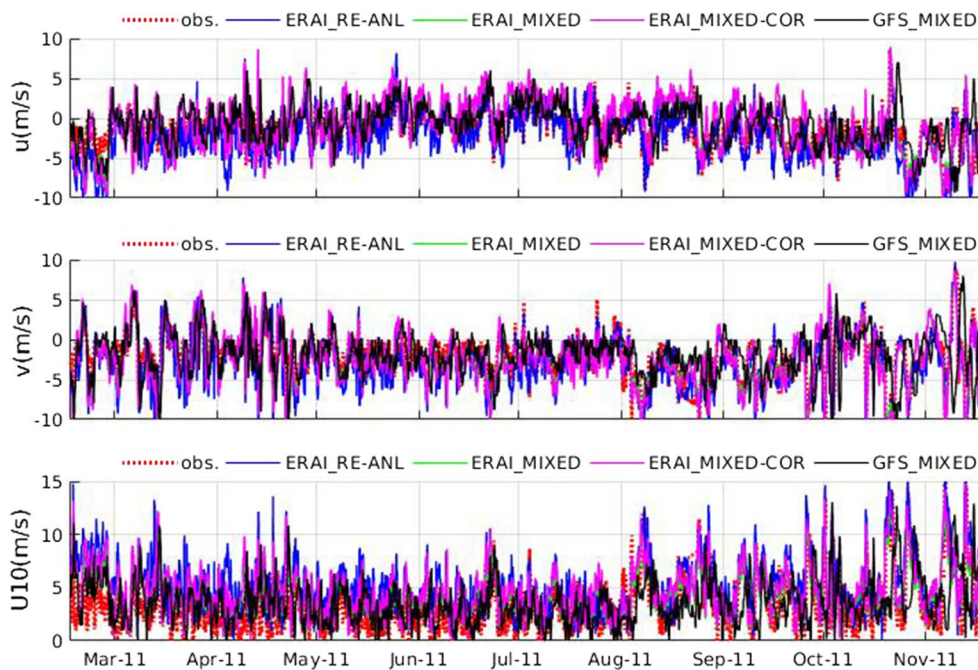
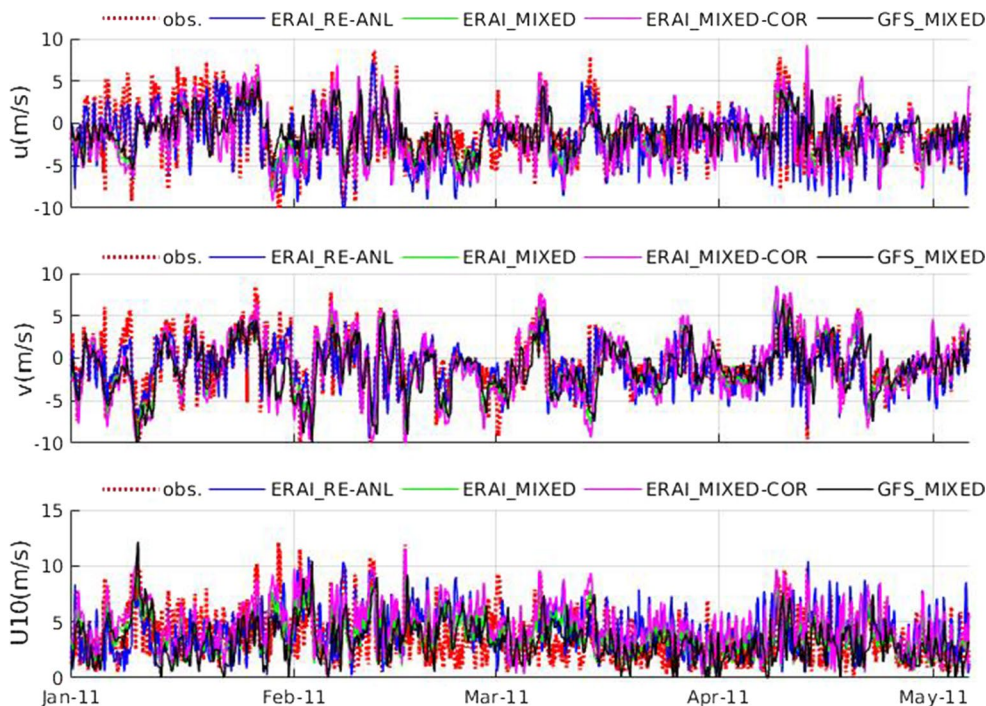


Fig. 5 Comparison of the wind components of u and v , and $U10$ from the observation and ERAI_RE-ANL, ERAI_MIXED, ERAI_MIXED-COR and GFS_MIXED data nearshore buoy (KB)



The statistical parameters used for validating wind datasets are presented in Table 2 and shown in Fig. 3a–d. The correlation coefficient (CC) for re-analysis and mixture of re-analysis/forecast dataset are very close together at 0.7. Based on the negative biases, the ERAI products underestimated wind velocities. Applying modification factors suggested by Mazaheri et al. (2013) has improved mean bias value. However, the mixed version of re-analysis/forecast

wind data provided better statistical parameters. The lowest root means square errors (RMSE) and scatter index (SI) are found as 1.60 m/s and 0.28 for ERAI_MIXED datasets. Nevertheless, this implies that ERAI_MIXED dataset outperforms other ERAI datasets. The GFS_MIXED wind dataset overestimated wind values throughout the SBC.

Rusu and Onea (2013) compared the AVISO remotely sensed dataset with ERAI at fifteen fixed points along

Table 3 Statistical parameters in terms of mean bias error (MBE) and root mean square error (RMSE), scatter index (SI), correlation coefficient (CC) and index agreement (IA) at offshore buoy (DB) and nearshore buoy (KB)

Buoy position	ERA1_RE-ANL			ERA1_MIXED			ERA1_MIXED-COR			GFS_MIXED		
	u	v	U10	u	v	U10	u	v	U10	u	v	U10
DB												
MBE (m/s)	-0.13	-0.01	0.08	-0.22	-0.27	0.79	-0.29	-0.50	1.22	-0.88	-1.02	1.80
RMSE (m/s)	1.57	2.06	2.03	1.35	1.43	1.53	1.48	1.58	1.68	1.57	1.73	1.87
SI	0.57	-1.09	0.57	0.43	-0.71	0.43	0.47	-0.78	0.47	0.52	-0.80	0.52
CC	0.76	0.66	0.21	0.89	0.88	0.69	0.89	0.88	0.69	0.84	0.86	0.68
IA	0.86	0.80	0.50	0.93	0.94	0.80	0.92	0.93	0.78	0.87	0.90	0.74
KB												
MBE (m/s)	-0.04	-0.21	-0.40	-0.17	-0.12	0.16	-0.44	-0.28	0.94	-0.59	-0.41	0.40
RMSE (m/s)	1.19	1.52	1.70	1.32	1.33	1.50	1.59	1.59	1.80	1.55	1.25	1.72
SI	0.46	-1.64	0.46	0.40	-1.96	0.40	0.49	-2.35	0.49	0.46	-1.73	0.46
CC	0.81	0.84	0.31	0.85	0.90	0.44	0.85	0.90	0.44	0.86	0.88	0.38
IA	0.88	0.91	0.58	0.92	0.95	0.67	0.91	0.94	0.65	0.91	0.93	0.64

the Caspian Sea where five points were in the SBC. They found the values of MBE, RMSE, SI and CC as 0.12 m/s, 1.26 m/s, 0.28 and 0.83 in a position which are similar to values found in at DB buoy. However, those results were based on one station point in SBC while spatially extensive area was used for comparisons in the present work.

4.2 Wind data analysis

Time series of wind velocity are presented in Fig. 4 for offshore station and in Fig. 5 for nearshore buoy. At offshore location (Fig. 4), the wind speed varied from zero to 15.94 m/s with a mean of 3.56 m/s. The corresponding values were from zero to 13.04 m/s with a mean of 3.64 for the ERA1_RE-ANL, from 0.02 up to 13.46 m/s with a mean of 4.36 m/s for the ERA1_MIXED, from 0.02 to 14.81 m/s with a mean of 4.80 m/s for the ERA1_MIXED-COR, and from 0.10 to 17.33 m/s with a mean of 5.43 m/s for the GFS_MIXED datasets. The nearshore buoy (KB) has been located nearly 150 km far from DB station, 2 km away from the coastline. Although the buoy has been operated from January 2010 to June 2011, but the last 5-month measurements were available for this study. At the nearshore buoy location (Fig. 5), where the wind speed measurements ranged from 0.2 to 12.1 m/s with a mean of 3.72 m/s, the corresponding values were from zero to 12.14 m/s with a mean of 3.32 from the ERA1_RE-ANL, from 0.18 to 9.65 m/s with a mean of 3.88 m/s from the ERA1_MIXED, from 0.21 to 11.58 m/s with a mean of 4.66 m/s for the ERA1_MIXED-COR, and from 0.21 to 10.83 m/s with a mean of 4.12 m/s for the GFS_MIXED datasets, respectively.

The statistical indices for the ERA1_RE-ANL, ERA1_MIXED, ERA1_MIXED-COR, and GFS_MIXED wind datasets are presented in Table 3 and shown in Figs. 6 and 7.

For offshore location (DB), according to the negative biases, it can be noticed that all ERAI and GFS datasets underestimated the wind velocity components. The RMSE varies in the range of 1.35–1.57 for u component, and 1.43–2.06 for v component, and 1.48–2.03 for U10. The best index of agreements, IA (0.93, 0.94 and 0.80 for u, v and U10), was resulted for the ERA1_MIXED dataset. The ERA1_MIXED also provided the lowest RMSE and SI values among all datasets at the offshore position, which implies its higher accuracy. Generally, datasets overestimated the wind velocity at the DB buoy location, especially before June. For the nearshore buoy location (Fig. 7), the RMSE and SI values implied that ERA1_MIXED provided a more accurate estimate of wind velocity than other datasets. The RMSE values for KB location are slightly less than DB, and GFS_MIXED and ERA1_MIXED datasets were the most successful datasets.

The overall conclusion is the fact that ERAI significantly underestimates the wind speed when compared to measured data at buoys locations. Mazaheri et al. (2013) also obtained the similar conclusion for the ECMWF wind field. However, in the present study, the result of the comparison does not support the good performance of the ERA1_MIXED-COR wind field.

The wind frequency distributions from measurements and datasets are presented in Table 4. Hourly records during Feb–Nov 2011 for offshore location and during Jan–May 2011 for nearshore stations are used. According to Beaufort Wind Scale, the dominant condition is between light air and gentle breeze conditions. However, the most frequent wind is light breeze condition based on the observation and GFS_MIXED data, and gentle breeze from ERAI datasets.

The directional distribution of wind vectors is depicted in Fig. 8a, b for offshore and nearshore buoys. For the point

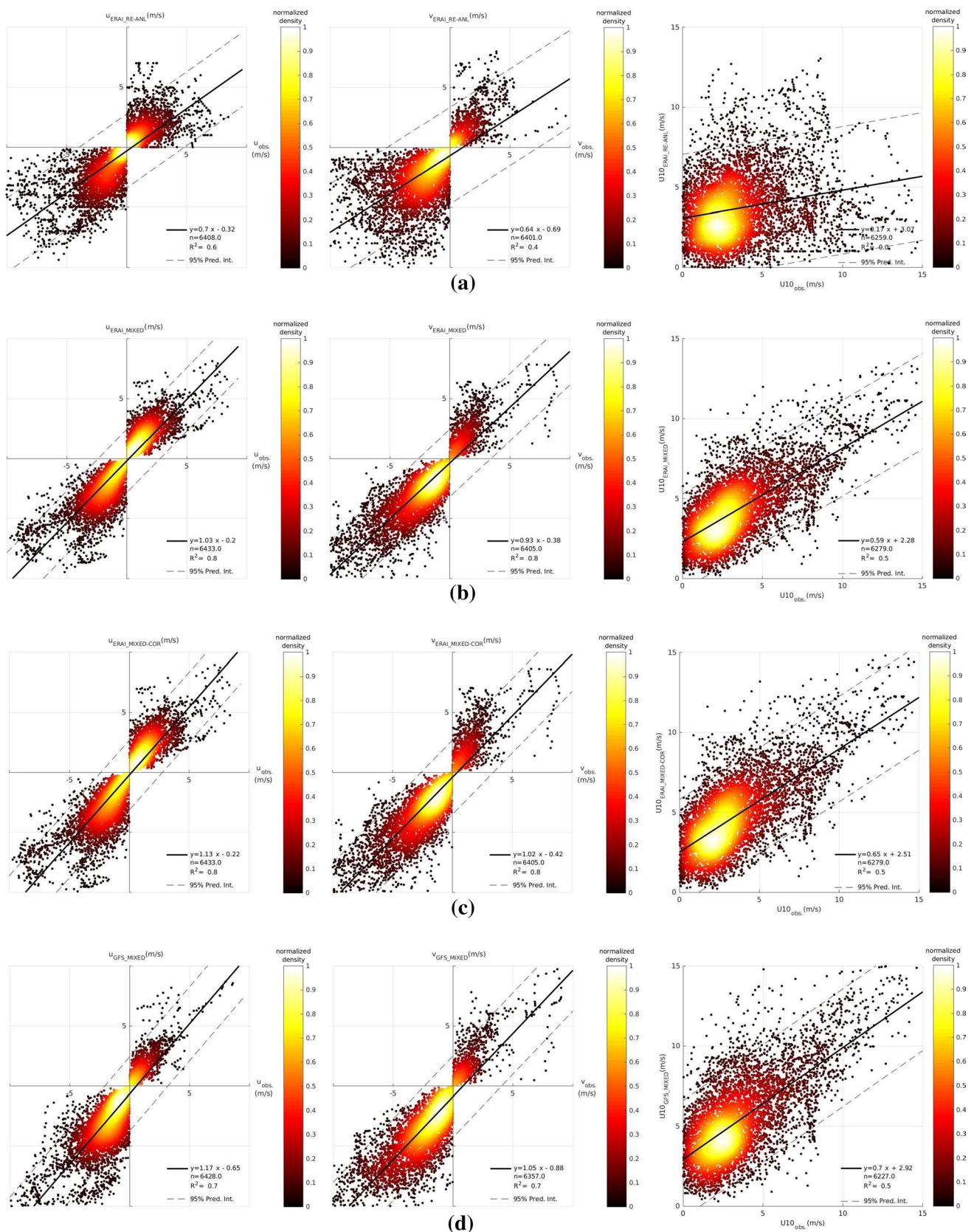


Fig. 6 Scatter plot for wind components of u and v, and U10 from the observation and **a** ERAI_RE-ANL, **b** ERAI_MIXED, **c** ERAI_MIXED-COR and **d** GFS_MIXED data at offshore buoy (DB)

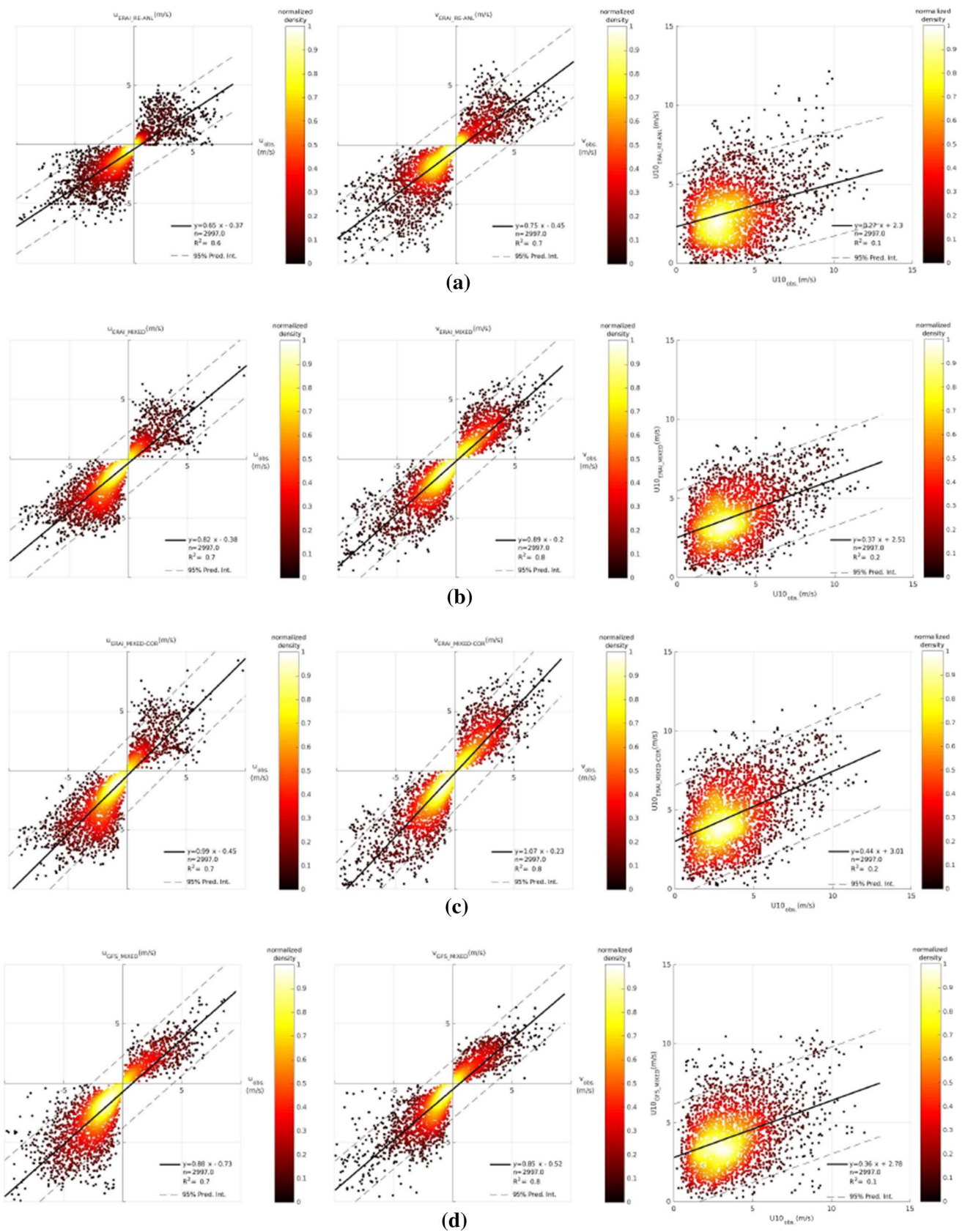


Fig. 7 Scatter plot for wind components of u and v, and U10 observation and **a** ERAI_RE-ANL, **b** ERAI_MIXED, **c** ERAI_MIXED-COR and **d** GFS_MIXED data at nearshore buoy (KB)

Table 4 Beaufort wind force scale from the buoy wind data and (a) ERAI_RE-ANL, (b) ERAI_MIXED, (c) ERAI_MIXED-COR and (d) GFS_MMIXED datasets at offshore and nearshore buoy locations

	Beaufort wind force scale							
	Calm	Light air	Light breeze	Gentle breeze	Moderate breeze	Fresh breeze	Strong breeze	High wind
U10 (m/s)	<0.3	0.3–1.5	1.5–3.3	3.3–5.5	5.5–7.9	7.9–10.7	10.7–13.8	>13.8
DB								
Buoy	2.5	15	36.3	23.3	9.9	5.8	1.4	0.3
(a)	0.1	6	28.8	39.4	18.9	5.5	1.2	0
(b)	0.1	2.9	17.8	39.1	24.2	12	3.2	0.7
(c)	0.1	4.5	23.7	38.8	23	7.8	2	0.2
(d)	1.5	11.6	36.5	34.1	12	3.7	0.6	0
KB								
Buoy	0.1	11.2	37.5	34.8	12	4.1	0.3	0
(a)	0.2	6.5	32.8	42.3	16.8	1.3	0	0
(b)	0.2	5.9	30.2	42	18.3	3.4	0	0
(c)	0.1	4	21.6	42	26	6	0.2	0
(d)	1.4	14.9	37.8	34.8	9.5	1.5	0.2	0

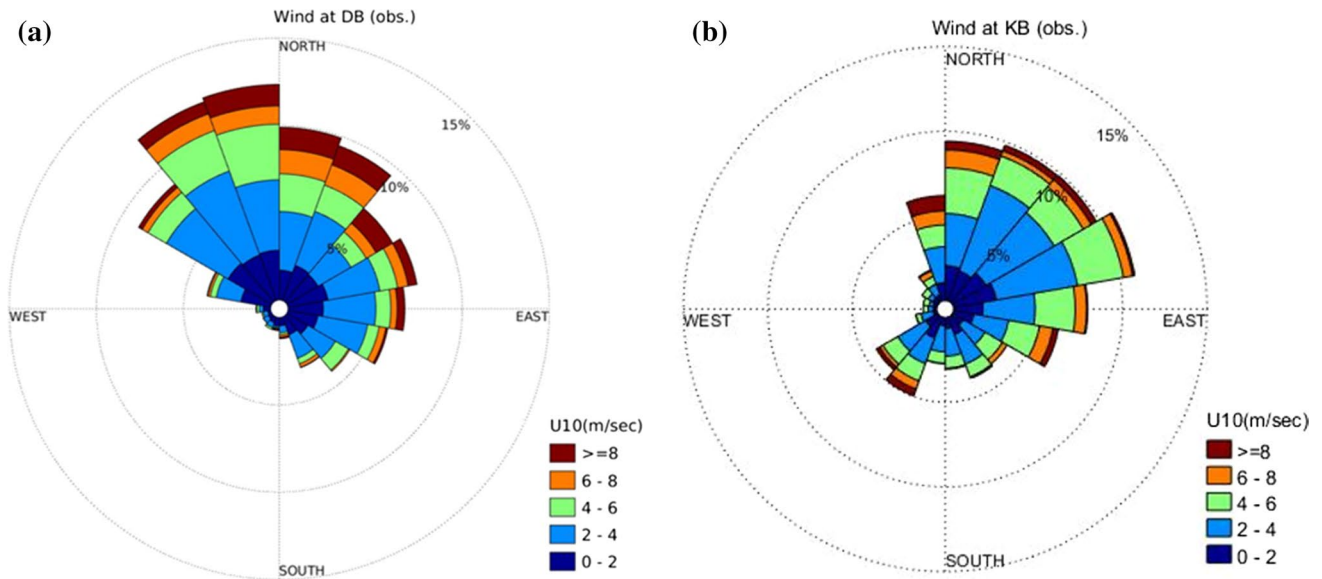


Fig. 8 Wind roses for the DB and KB location based on buoy data. Analysis performed for February to November 2011 in DB location and for February to May 2011 in KB location

located in the center of SBC (DB), it can be noticed that the northwesterlies and easterlies are dominant (Fig. 8a). However, the strongest winds are coming from northeast. For KB location, wind rose highlighted the importance of the northwest to east wind directions (Fig. 8b). The winds never exceed 10 m/s in both locations; the frequency of wind speed higher than 9 m/s was 2–6%. Rusu and Onea (2013) suggested north-eastern dominant wind conditions for north and west of the SBC location. Regarding the

location of the buoy (KB), the winds are strongly influenced by the orographic feature of SBC, including Alborz and Caucasus mountains in the south and west of SBC.

Comparison of time series of wind speed and direction obtained from ERAI and GFS dataset with remotely sensed data from CERSAT and observations at offshore and nearshore buoys supported the use of ERAI_MIXED dataset for wave simulations in SBC.

Table 5 Wave statistical parameters in terms of mean bias error (MBE), root mean square error (RMSE), scatter index (SI), correlation coefficient (CC) and index agreement (IA) at offshore buoy (DB) and nearshore buoy (DB) using (a) ERAI_RE-ANL, (b) ERAI_MIXED, (c) ERAI_MIXED-COR and (d) GFS_MIXED wind data

	Station	DB					KB					
		MBE	RMSE	SI	CC	IA	MBE	RMSE	SI	CC	IA	
H_s	Komen											
	(a)	-0.33	0.35	0.44	0.24	0.42	0.07	0.27	0.48	0.76	0.86	
	(b)	-0.22	0.20	0.26	0.88	0.86	-0.13	0.18	0.33	0.76	0.82	
	(c)	-0.12	0.25	0.32	0.87	0.91	-0.02	0.23	0.41	0.79	0.88	
	(d)	-0.05	0.27	0.35	0.87	0.93	-0.20	0.22	0.39	0.59	0.68	
	Janssen											
	(a)	0.26	0.60	0.76	0.21	0.48	0.75	0.49	0.88	0.72	0.60	
	(b)	0.43	0.36	0.46	0.87	0.85	0.40	0.34	0.61	0.72	0.71	
	(c)	0.60	0.44	0.56	0.87	0.79	0.60	0.41	0.74	0.76	0.64	
	(d)	0.74	0.51	0.64	0.86	0.75	0.30	0.39	0.70	0.54	0.65	
	T_p	Komen										
		(a)	-0.77	1.30	0.26	0.16	0.47	1.24	1.01	0.27	0.62	0.64
(b)		-0.50	0.89	0.18	0.76	0.84	0.64	0.99	0.27	0.51	0.67	
(c)		-0.25	0.93	0.19	0.77	0.87	0.94	1.03	0.28	0.55	0.65	
(d)		-0.23	0.86	0.17	0.80	0.89	0.35	1.11	0.30	0.28	0.56	
Janssen												
(a)		0.33	1.36	0.27	0.20	0.51	2.56	1.23	0.33	0.58	0.49	
(b)		0.65	0.99	0.20	0.74	0.82	1.74	1.24	0.33	0.48	0.52	
(c)		0.91	1.09	0.22	0.73	0.79	2.00	1.27	0.34	0.54	0.52	
(d)		0.94	1.05	0.21	0.74	0.79	1.41	1.15	0.31	0.31	0.46	

4.3 Wave modeling

Conventional wave data are scarce in the southern part of Caspian Sea. Fortunately, in the last decade, a few field investigations were carried out using the buoy and bottom-mounted acoustic instruments. For this study, measured wave data have been collected from one offshore buoy (DB) located in the middle of SBC operated from February to November 2011, one mid-shelf buoy (KB) near Kiashahr Port deployed from January to May 2011 and an ADCP bottom mounted (AA) near Anzali port from 27 June to 10 July 2011. Two observation data from buoys were used for calibrating the regional SWAN model and the last is used in the local nested grid. For both buoys, only bulk wave parameters including significant wave height (H_s), peak period (T_p) and direction were available at 1 h intervals.

As mentioned in Sect. 4.2, evaluation of different wind datasets implied that the ERAI_MIXED dataset was more consistent with the measurement data. It can also be confirmed by wave simulation, when different wind data are forced to model. To avoid any complexity, SWAN model using default setting was evaluated: Two different exponential wind growth formulations of Komen (WAM cycle 3) and Janssen (WAM cycle 4) were considered for wave generation in combination with the Komen whitecapping dissipation. Statistical parameters presented in Table 5 showed that the Komen formulation was more successful than Janssen

formulation. Since the ERAI_MIXED dataset resulted in lower values of RMSE and SI for wave at both DB and KB stations, it can be concluded that this dataset should be used as the main forcing over the Caspian Sea.

In the next step, model calibration was carried out in order the tune wave generation and whitecapping parameters. Hartgerink (2005) used the Komen formulation with C_{ds2} values of $2.38e-5$ (default), $1e-5$ and $5e-5$ and found that the default value outperforms the others when $\delta=1$ was used. Rusu and Onea (2013) used the Janssen formulation for exponential wind growth with $C_{ds1}=3.2$ and $\delta=0.55$, and Van der West-Huysen formulation for whitecapping. Hadadpour et al. (2014) and Kamranzad et al. (2016) used the Komen formulation with default values. The effects of changing the whitecapping coefficients at DB station are shown in Fig. 9 as direct comparison (Fig. 9a) and scatter plots (Fig. 9b, c) (ERAI_MIXED wind data are forced to model).

Evaluation of different whitecapping dissipation coefficients shows that Komen formulation with default value generates convenient results; however, the use of $C_{ds}=1.3e-5$ resulted in a better agreement to measurements. The statistical indices for model performance using different whitecapping dissipation (cds) are presented in Table 6.

The comparison between SWAN results with measurements is shown in Figs. 10, 11, and 12. At the offshore

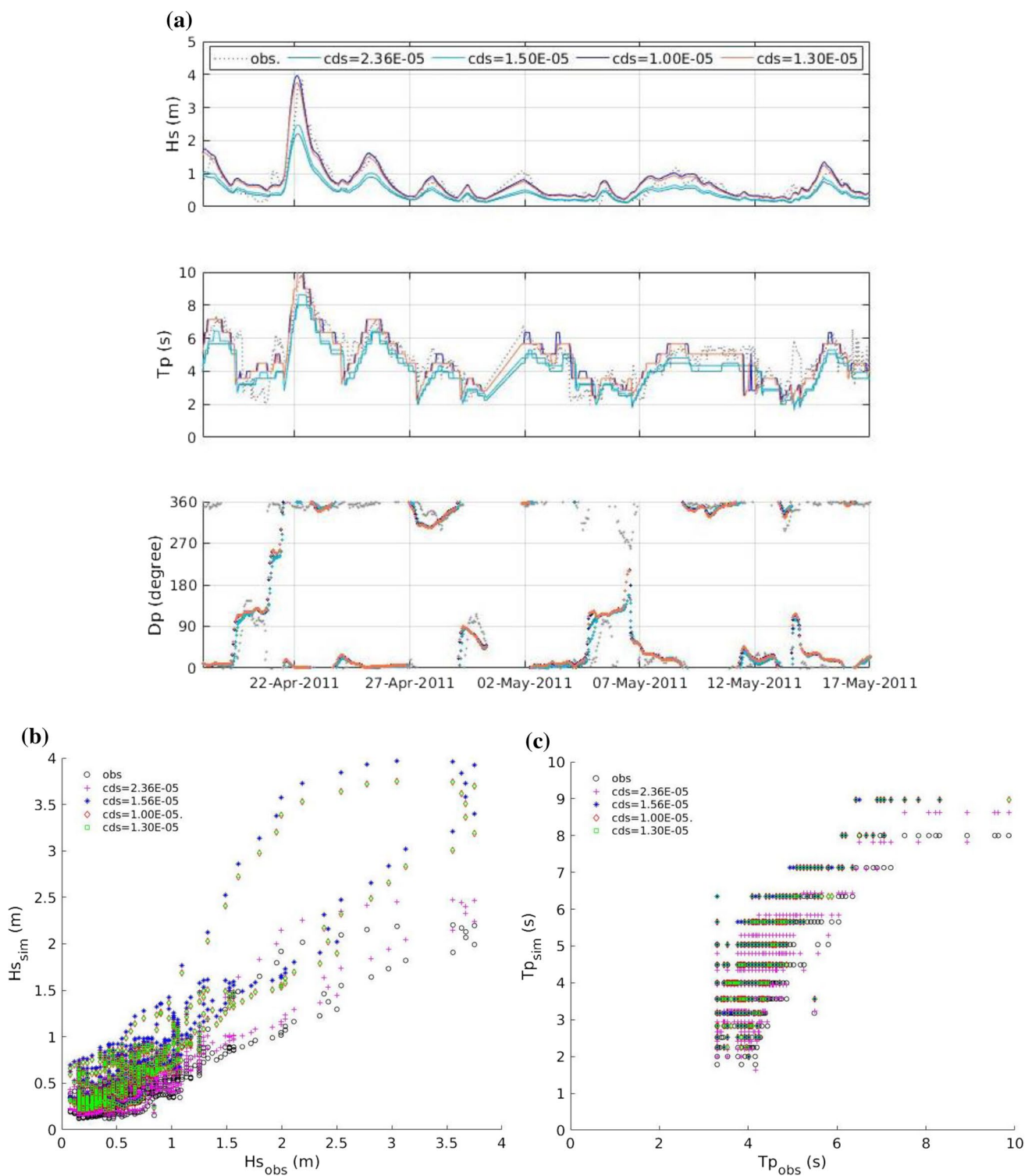


Fig. 9 a Comparison and scatter plot for wave characteristics with different rate of whitecapping dissipation using Komen formulation and ERAI_MIXED wind data, b scatter plot from simulated and

observation wave height and c scatter plot from simulated and observation peak period

location, the results revealed consist trends of the model results and the measurements but also suggest a poor performance of model in capturing H_s and T_p values correctly. The

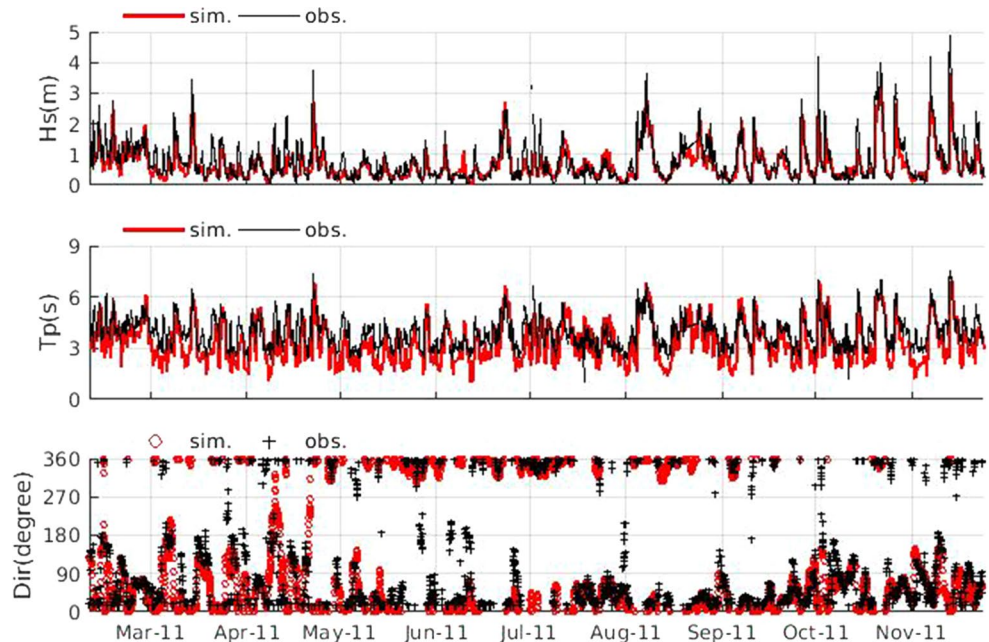
wave heights values produced by the model at DB vary in the range of 0.07–4.66 m with the mean and standard deviations of 0.68 and 0.52 m. In contrast, the maximum measured H_s

Table 6 Statistical parameters for whitecapping calibration on H_s and T_p , in terms of mean bias error (MBE), root mean square error (RMSE), scatter index (SI), correlation coefficient (CC) and index agreement (IA), mean, and standard deviation (SD) in the offshore location

	Whitecapping dissipation coefficient (Cds1)			
	2.30E-05	1.50E-05	1.00E-05	1.30E-05
H_s (m)				
MBE	-0.22	-0.16	0.08	0.03
RMSE	0.13	0.14	0.25	0.23
SI	0.20	0.22	0.39	0.37
CC	0.92	0.92	0.91	0.90
IA	0.84	0.89	0.95	0.95
Mean	0.41	0.47	0.72	0.67
SD	0.55	0.55	0.55	0.55
T_p (s)				
MBE	9.15	3.28	10.76	10.35
RMSE	4.94	0.74	4.83	4.80
SI	6.02	0.90	5.90	5.86
CC	0.82	0.80	0.83	0.83
IA	0.44	0.40	0.44	0.44
Mean	9.97	0.82	11.59	0.82
SD	8.56	0.92	0.91	0.91

from the buoy exceeds 4.88 m with the mean value of 0.74 m and the standard deviation of 0.56 m. Also, the peak wave period varies from 1.26 to 9.98 s in model results. The mean and standard deviation are 4.63 and 1.5 s, respectively. The measured values for T_p vary from 0.34 to 14.2 s with mean values of 4.9 s and standard deviation of 1.5 s.

Fig. 10 Direct comparison of the wave parameters H_s and T_p , and wave direction between the observation (solid, bobble) and ERAI_MIXED (dotted and plus symbols) data at offshore buoy (DB)



Statistical wave parameters and directional spreading are presented in Table 7 and shown in Fig. 13. The bias errors for H_s varied from -2.82 to -1.26 m, with value of -0.12 m for the MBE. The negative values of the mean bias error for both significant wave height and wave period suggest a significant underestimation at the offshore buoy. This is consistent with the results of Jafari et al. (2014). The discrepancy was more significant in early July when v-component of wind forcing was significantly different from the measurements. For the root means square (RMSE) and SI, the related values are found as 0.25 m and 0.36 with the correlation coefficients (CC) of 0.88. For the peak period (T_p), the MBE was found as -0.36 s, while the RMSE value was 0.98 s, and the SI and the CC values were 0.21 s and 0.79, respectively.

The cumulative frequencies of the wave results at offshore station implied that the simulated wave height about 88% of time was less than 1 m, where only 2.1% was higher than 2 m. Also, the wave period was less than 47.8% below 3 s and 52.2% above 3 s. At the nearshore buoy station, about 5.2% of time, the wave height was higher than 1 m and 10% of the waves occurs with less than 3 s periods and slightly less than 5% occurs with higher than 8 s.

Comparison of wave characteristics from buoy data with model results (Fig. 13a) showed the values of linear regression (R^2) found at 0.8 and 0.6 for H_s and T_p and the slopes of the regression lines are lower than 1. These are implied that the model underestimated H_s and T_p ; however, the RSME values suggested a good consistency for wave height and wave period except for some specific events.

At the Kiashahr buoy (KB), the values of linear regression (R^2) were found at 0.6 and 0.3 for H_s and T_p (Fig. 13b).

Fig. 11 Direct comparison of the wave parameters H_s and T_p , and wave direction between the observation (solid, bobble) and ERAI_MIXED (dotted and plus symbols) data on offshore buoy (KB)

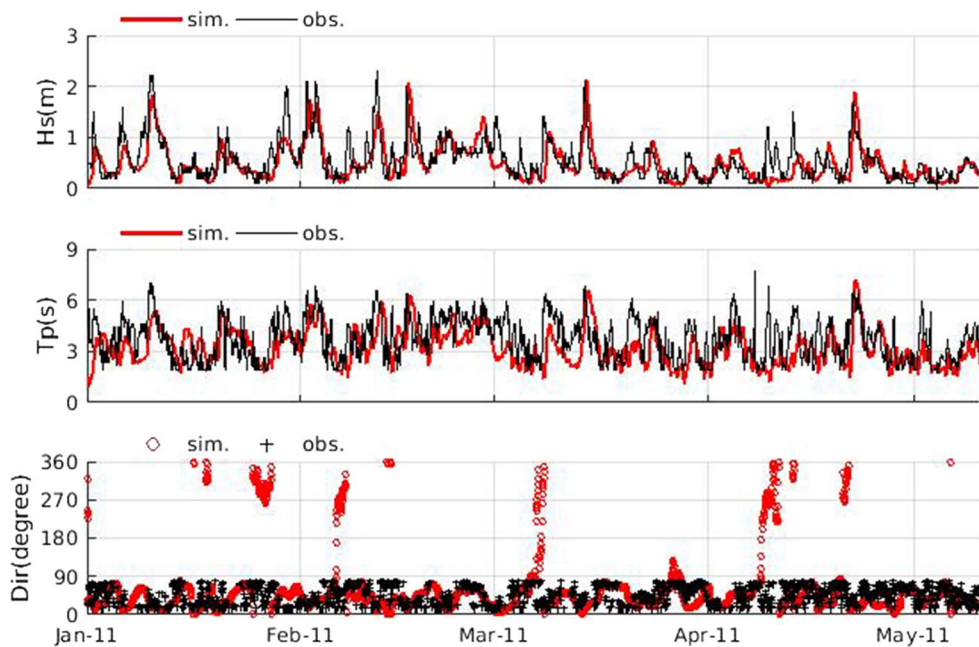


Fig. 12 Direct comparison of the wave parameters H_s and T_p , and wave direction between the observation (solid, bobble) and ERAI_MIXED (dotted and plus symbols) data on ADCP location (AA)

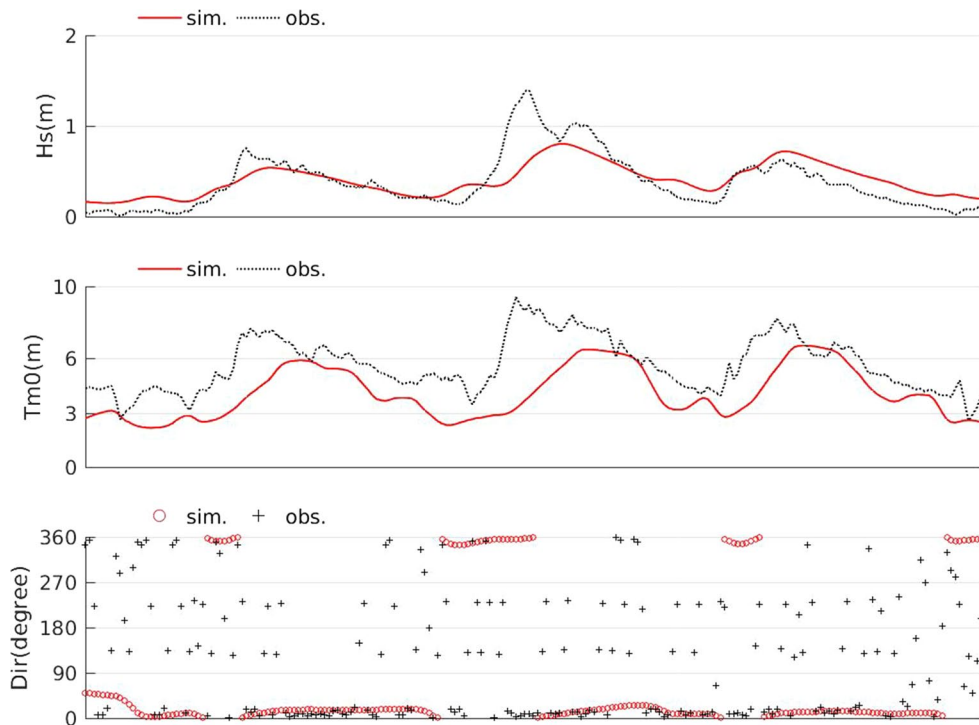


Table 7 Hourly statistics for the wave characteristics in terms of mean bias error (MBE), root mean square error (RMSE), scatter index (SI), correlation coefficient (CC) and index agreement (IA) on offshore buoy (DB), nearshore buoy (KB) and ADCP (AA) locations

	DB		KB		AA	
	H_s (m)	T_p (s)	H_s (m)	T_p (s)	H_s (m)	T_p (s)
MBE	-0.05	0.8	0.08	1.13	0.02	0.03
RMSE	0.23	1.09	0.29	1.15	0.1	1.42
SI	0.47	0.24	0.46	0.24	0.27	0.25
CC	0.76	0.51	0.79	0.54	0.81	0.67
IA	0.87	0.65	0.87	0.63	0.82	0.8

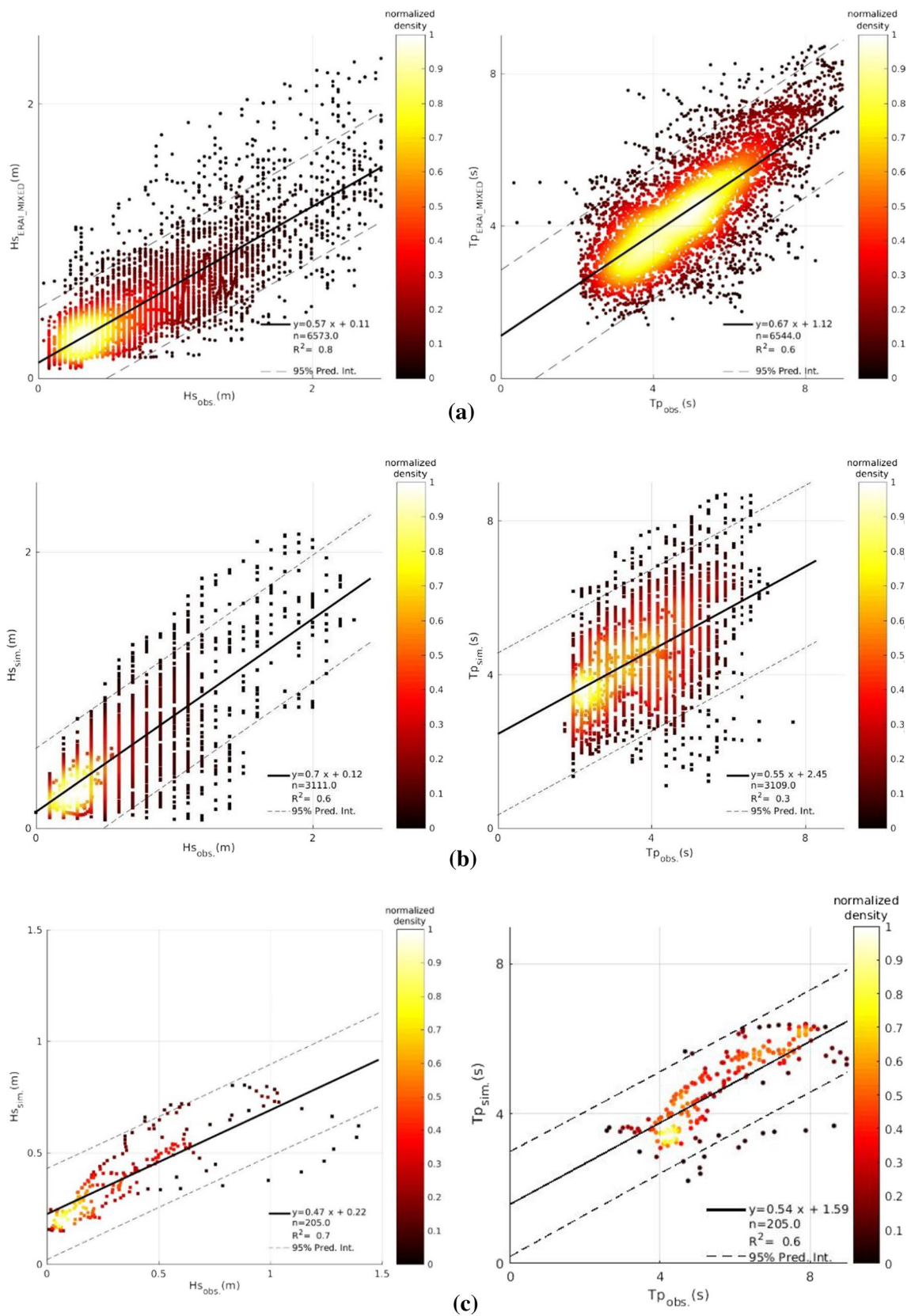


Fig. 13 Scatter plot for wave characteristics by comparing the observation data and simulated results using ERAI_MIXED wind data forcing **a** on offshore buoy (DB), **b** on nearshore buoy and **c** ADCP station (AA)

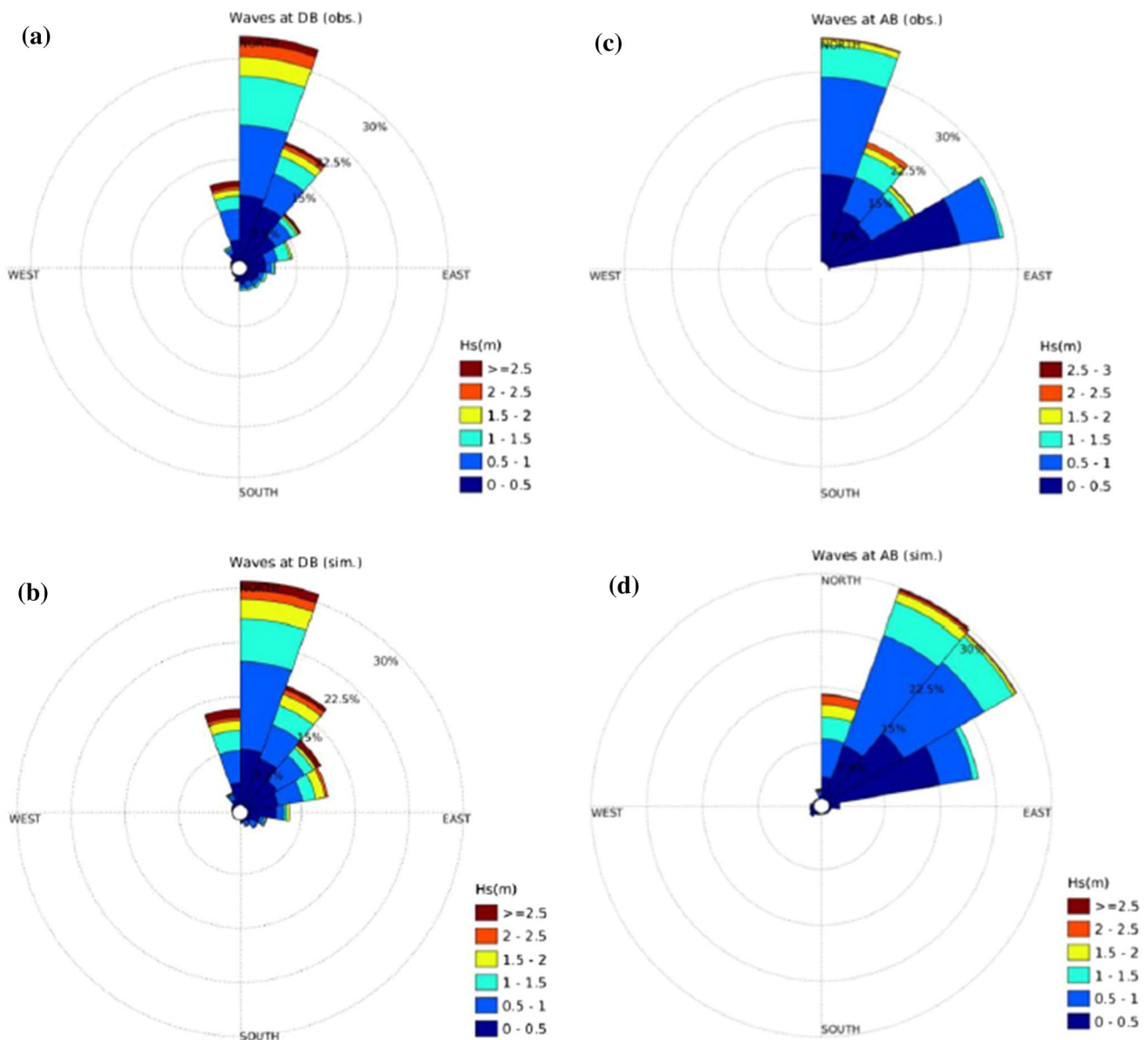


Fig. 14 Wave roses for the **a** offshore (DB) and **b** nearshore (KB) location based on buoy data. Analysis performed for Feb–Nov 2011 in DB location and for Jan–May 2011 in KB location

In similarity of offshore location, the slopes of the regression lines are slightly lower than 1, suggesting that model result underestimate the nearshore location data.

Direct comparisons of the wave characteristics at ADCP location revealed a poor trend consistency between the model results and observation. In both locations, waves are distributed with the values of H_s less than 1 m. Over 80% of the time, the waves are observed at wave height of less than 1 m. The observations always are found at 80% with lower than 1 m wave height and nearly up to 3% are found above 2 m. These conditions indicate that the SBC usually has moderate to low conditions. Rusu and Onea (2013) found the contribution of 98% with less than 2 m

height for summer and 87% during winter. Waves in the enclosed water bodies are dominantly generated by winds and Caspian Sea.

Observed and simulated wave roses are presented in Fig. 14. At offshore location, waves are coming from the north to east direction and, in fact, they are mainly coming from the north sector (Fig. 14a). Simulation results (Fig. 14b) revealed the same pattern at DB point, which is also confirmed by observations. At nearshore buoy location, the waves are dominantly coming from the north and east (Fig. 14c). The model overestimated the north-east components and underestimated the north and east components as presented in Fig. 14d.

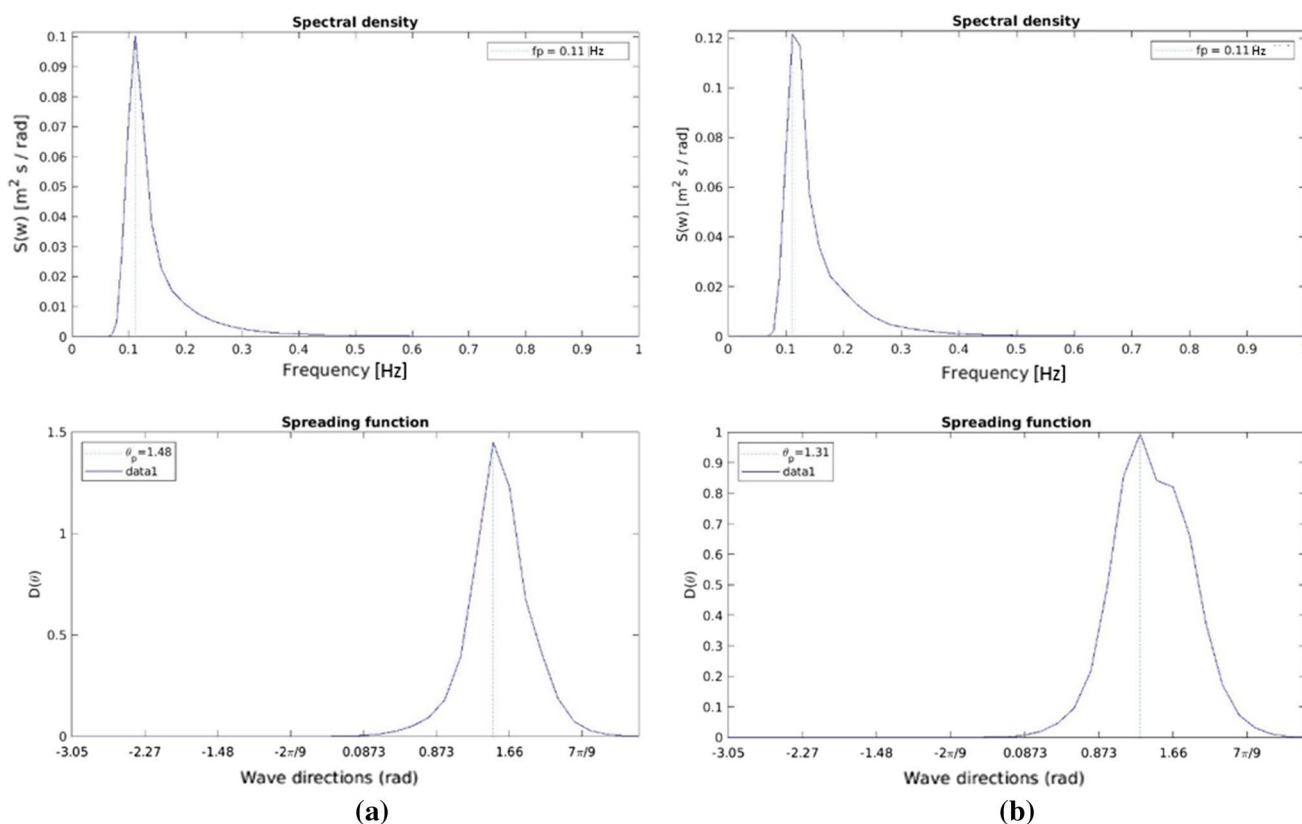


Fig. 15 Wave spectra for two consecutive events occurred at **a** March and **b** August at the offshore buoy location (DB)

The spectral information during two high energy events is shown in Fig. 15. It is clear from both wave spectrum and its direction spreading that high energy events are not bimodal at SBC; therefore, the model performance can be evaluated effectively using bulk wave parameters such as H_s and T_p .

5 Conclusions

High resolution ERA-Interim (ERA-I) wind forcing is evaluated in the southern basin of Caspian Sea (SBC) for the wave generation. The SWAN model was used to simulate the waves using two nested layer grids. The accuracy of the wind forcing significantly affects the performance of the model. Such wind data can be achieved from several resources such as remotely sensed data and global weather forecast system datasets. In the present study, mixed re-analysis and forecast ERA-Interim (ERA-I) dataset are evaluated to simulate wave condition in the SBC. The wind data were compared with CERSAT wind data, and the same process was repeated for GFS mixed re-analysis/forecast wind data. The results revealed a fairly good agreement between satellite-derived data and ERAI-MIXED datasets. However, underestimation of the

wind speed was quiet evidence. This wind dataset was used as forcing for SWAN model to simulate the wave characteristics. Three measurement stations including two met-ocean buoys and one ADCP were used to evaluate the wave model performance. The latest measurement data are published for the first time in this study.

Since ERAI dataset has been critiqued for its underestimation of the wind velocity, some local correction coefficients were suggested in previous studies. The direct comparison of the wind data with satellite-derived wind speed, and the performance of SWAN using such wind data did not support using such correction factors.

Although the uncertainty in the wind data affects the wave model results, the SWAN provided acceptable bulk wave characteristics using ERAI-MIXED wind data. The analysis results showed a good agreement between observation and model results for both significant wave height and wave period except during some extreme events. The results calculated from the observation and ERAI data showed that ERAI slightly overestimated the bulk wave parameters in the offshore station and underestimated it close to nearshore buoy. Finally, the quantitative evaluation of directional distribution of wind conditions indicated the moderate to low energy conditions at SBC.

Acknowledgements This work was partially supported by the Iranian National Institute for Oceanography and Atmospheric Sciences (INIOAS) under nearshore modeling program. Authors also wish to thank John Warner for making the COAWST code available and to Kate Kshedstrom for her PYROMS code.

References

- Arpe K, Leroy SA (2007) The Caspian Sea Level forced by the atmospheric circulation, as observed and modelled. *Quat Int* 173:144–152
- Battjes J, Janssen J (1978) Energy loss and set-up due to breaking of random waves. In: Proceedings of 16th international conference on coastal engineering, Hamburg, Germany, 27 August–3 September 1978. ASCE
- Beji S, Battjes J (1993) Experimental investigation of wave propagation over a bar. *Coast Eng* 19(1):151–162
- Booij N, Holthuijsen L, Ris R (1996) The “SWAN” wave model for shallow water. In: Proceedings of 25th international conference on coastal engineering, Orlando, Florida, US, 2–6 September 1996. ASCE
- Booij N, Ris R, Holthuijsen LH (1999) A third-generation wave model for coastal regions: 1. Model description and validation. *J Geophys Res Oceans* 104(C4):7649–7666
- Bouws E, Komen G (1983) On the balance between growth and dissipation in an extreme depth-limited wind-sea in the southern North Sea. *J Phys Oceanogr* 13(9):1653–1658
- Cavaleri L, Rizzoli PM (1981) Wind wave prediction in shallow water: theory and applications. *J Geophys Res Oceans* 86(C11):10961–10973
- Collins JJ (1972) Prediction of shallow-water spectra. *J Geophys Res* 77(15):2693–2707
- Golshani A, Taebi S, Chegini V (2007) Wave hindcast and extreme value analysis for the southern part of the Caspian Sea. *Coast Eng J* 49(04):443–459
- Graham C, Cardone V, Ceccacci E, Parsons M, Cooper C, Stear J (2002) Challenges to wave hindcasting in the Caspian Sea. In: Paper presented at proceedings of 7th international workshop on wave hindcasting and forecasting (Canada), Citeseer
- Hadadpour S, Moshfeghi H, Jabbari E, Kamranzad B (2013) Wave hindcasting in Anzali, Caspian Sea: a hybrid approach. In: Conley DC, Masselink G, Russell PE, O’Hare TJ (eds) Paper presented at proceedings of 12th international coastal symposium, Plymouth, England. *Journal of Coastal Research*, Special issue no 65, pp 237–242
- Hadadpour S, Etemad-Shahidi A, Jabbari E, Kamranzad B (2014) Wave energy and hot spots in Anzali port. *Energy* 74:529–536
- Hartgerink P (2005) Analysis and modelling of wave spectra on the Caspian Sea. TU Delft, Delft University of Technology, Delft
- Hasselmann K (1974) On the spectral dissipation of ocean waves due to white capping. *Bound Layer Meteorol* 6(1–2):107–127
- Hasselmann K, Barnett T, Bouws E, Carlson H, Cartwright D, Enke K, Ewing J, Gienapp H, Hasselmann D, Kruseman P (1973) Measurements of wind-wave growth and swell decay during the Joint North Sea Wave Project (JONSWAP) Rep. Deutsches Hydrographisches Institut, Hamburg
- Hasselmann K, Allender JH, Barnett TP (1985) Computations and parameterizations of the nonlinear energy transfer in a gravity-wave spectrum. Part II: parameterizations of the nonlinear energy transfer for application in wave models. *J Phys Oceanogr* 15(11):1378–1391
- Ibrayev R, Özsoy E, Schrum C, Sur H (2010) Seasonal variability of the Caspian Sea three-dimensional circulation, sea level and air-sea interaction. *Ocean Sci* 6:311–329
- Jafari E, Alaee MJ, Pattiaratchi CB, Nemati MH, Farhand A (2014) Evaluation of the ECMWF era-interim wind data for numerical wave hindcasting in the Caspian Sea. *Coast Eng Proc* 1(34):40
- Kamranzad B, Etemad-Shahidi A, Chegini V (2016) Sustainability of wave energy resources in southern Caspian Sea. *Energy* 97:549–559
- Komen G, Hasselmann K, Hasselmann K (1984) On the existence of a fully developed wind-sea spectrum. *J Phys Oceanogr* 14(8):1271–1285
- Lopatoukhin LJ, Boukhanovsky AV, Chernysheva ES, Ivanov SV (2004) Hindcasting of wind and wave climate of seas around Russia. In: Paper presented at 8th international workshop on wave hindcasting and forecasting, North Shore, Oahu, Hawaii, 14–19 November 2004
- Mazaheri S, Kamranzad B, Hajjivalie F (2013) Modification of 32 years ECMWF wind field using QuikSCAT data for wave hindcasting in Iranian Seas. *J Coast Res SI* 65:344–349
- Naseka A, Bogutskaya N (2009) Fishes of the Caspian Sea: zoogeography and updated check-list. *Zoosystematica Ross* 18(2):295–317
- Parzen E (1999) Stochastic processes. SIAM, Philadelphia
- Rusu E, Onea F (2013) Evaluation of the wind and wave energy along the Caspian Sea. *Energy* 50:1–14
- Wilks DS (2011) Statistical methods in the atmospheric sciences. Academic Press, Oxford
- Willmott CJ, Robeson SM, Matsuura K (2012) A refined index of model performance. *Int J Climatol* 32(13):2088–2094
- Zhao D, Toba Y (2001) Dependence of whitecap coverage on wind and wind-wave properties. *J Oceanogr* 57(5):603–616